PROCEEDINGS OF SPIE

SPIEDigitalLibrary.org/conference-proceedings-of-spie

Channel-first design of modulated polarimeters

Jiawei Song, Israel Vaughn, Andrey Alenin, Michael Gehm, J. Scott Tyo

Jiawei Song, Israel J. Vaughn, Andrey S. Alenin, Michael E. Gehm, J. Scott Tyo, "Channel-first design of modulated polarimeters," Proc. SPIE 10655, Polarization: Measurement, Analysis, and Remote Sensing XIII, 106550I (14 May 2018); doi: 10.1117/12.2309847

SPIE.

Event: SPIE Commercial + Scientific Sensing and Imaging, 2018, Orlando, FL, United States

Channel-first design of modulated polarimeters

Jiawei Song[a], Israel J. Vaughn[a], Andrey S. Alenin[a], Michael E. Gehm[b], and J. Scott Tyo[a]

[a]University of New South Wales Canberra, Canberra 2610 ACT, Australia
[b]Duke University, Durham, NC 27708, USA

ABSTRACT

Multi-domain modulated polarimeters combine carriers on different domains to exploit the bandwidth of the measurement system. However, the inevitable systematic errors in polarimeters will degrade their bandwidth performance, so we developed a new type of multi-domain modulated polarimeter. Compared with conventional polarimeters and our previous separable designs, this new type of system can avoid some of the negative effects (such as the emergence of extraneous channels) caused by the systematic errors. To illustrate the advantages and disadvantages of both systems, both types of Stokes polarimeters are designed based on the same channel structure and their performance is simulated under systematic errors.

Keywords: Polarimetry, Multi-domain Modulation, Fourier, Non-Separable

1. INTRODUCTION

Polarization is a basic property of light and it refers to the geometrical orientation of the electric field oscillations. Light from any source is polarized to some degree. Polarimetry is the study of estimating the extent to which the light is polarized, and it is valuable for remotely obtaining information from the scenes of interest. The polarizing effects of objects can be described by Mueller matrices which can be measured by active polarimeters, and the polarization states of light can be described by Stokes vectors which can be measured by passive polarimeters. Many different methods have been developed to measure Mueller matrices and Stokes vectors. Channeled polarimetry is a technique which measures polarimetric information by coding the incident light with carriers in spectral, temporal or spatial domains and then recovers desired polarimetric information from the modulation of those carriers. We denote the frequency space representation of the carriers *the system's channels*. These types of Stokes polarimeters were first introduced by Oka and Kato[1] and then extended to Mueller (active) polarimeter designs.[2–4] LaCasse's work[5] investigating the bandwidth in modulated polariemters and Alenin's work[6] investigating manupulation of channels in Fourier space then enabled proper treatment for multi-domain modulations. A multi-domain modulated polarimeter is a type of polarimeter that combines channel generation on different domains (e.g. space, time, wavelength, etc.) in order to extend the potential bandwidth of the polarimetric system.[4,7–12] Previously, multi-domain modulated polarimeters were designed using conventional elements with each element responsible for varying measurement conditions in a single domain. In this paper, we introduce a channel-first perspective for designing channel structures and demonstrate it on a new Stokes polarimeter design.

In polarimetry, the Stokes-Mueller formalism is commonly used to characterize the polarization measurement process. The polarization states of light can be fully described by Stokes vector.[13] The Stokes vector consists of four observables of the polarized field called the Stokes polarization parameters

$$\underline{\mathbf{S}} = \begin{bmatrix} S_0 \\ S_1 \\ S_2 \\ S_3 \end{bmatrix} = \begin{bmatrix} \left\langle E_{0x}^2 \right\rangle + \left\langle E_{0y}^2 \right\rangle \\ \left\langle E_{0x}^2 \right\rangle - \left\langle E_{0y}^2 \right\rangle \\ \left\langle 2E_{0x}E_{0y}\cos\delta \right\rangle \\ \left\langle 2E_{0x}E_{0y}\sin\delta \right\rangle \end{bmatrix}, \quad where\ S_0 > 0,\ S_0^2 \geq S_1^2 + S_2^2 + S_3^2 \tag{1}$$

In equation(1), $\langle . \rangle$ denotes time average, E_{0x}, E_{0y} are the amplitude of the electric field in the x and y directions, δ is the phase difference between the electric field of x and y direction, S_0 is proportional to the total intensity,

Further author information: (Send correspondence to J.S.)
J.S.: E-mail: jiawei.song@student.adfa.edu.au, Telephone: +61 (0)447 246 522

Polarization: Measurement, Analysis, and Remote Sensing XIII, edited by David B. Chenault, Dennis H. Goldstein, Proc. of SPIE Vol. 10655, 106550I · © 2018 SPIE · CCC code: 0277-786X/18/$18 · doi: 10.1117/12.2309847

S_1 is proportional to the prevalence of horizontal (0°) over vertical (90°) polarization, S_2 is proportional to the prevalence of +45° over −45° polarization, and S_3 is proportional to the prevalence of right circular over left circular polarization.

Mueller matrices are 4×4 matrices representing the linear transformations of an incident set of Stokes parameters and characterizing the polarization effects of different objects. The linear transformation of a set of Stokes parameters can be expressed as:

$$\underline{\mathbf{S}}_{out} = \underline{\underline{\mathbf{M}}} \cdot \underline{\mathbf{S}}_{in} \tag{2}$$

Optical detectors are typically insensitive to polarization of light, and S_0 is the only directly measurable Stokes parameter. Therefore, to measure the full Stokes vector, polarimeters need to derive the Stokes parameters from modulated carriers on the measured irradiance or radiance. From the view of communication theory, the carriers will generate channels that carry information about the light beam, and the original Stokes parameters will modulate those carriers, allowing recovery after channel un-mixing. The modulation and detection process in polarimeter can be expressed as:

$$S_0 = \underline{\mathbf{A}} \cdot \underline{\underline{\mathbf{M}}}_1 \cdot \underline{\underline{\mathbf{M}}}_2 \cdots \underline{\underline{\mathbf{M}}}_n \cdot \underline{\mathbf{S}}_{in} = \underline{\mathbf{A}}_s \cdot \underline{\mathbf{S}}_{in} \tag{3}$$

where $\underline{\underline{\mathbf{M}}}_n$ denotes the Mueller matrix of the nth modulating element, $\underline{\mathbf{A}}_s$ represents the analyzer vector of the system. Since only S_0 of the projected Stokes vector is detected, only the first row of the system Mueller matrix of the analyzer is used.

Since Mueller matrices are fourth order matrices and the analyzer vector is the first row of a Mueller matrix, for a Stokes polarimeter, Equation (3) can be rewritten as the dot product:

$$I_0 = S_0 = \underline{\mathbf{A}}_s \cdot \underline{\mathbf{S}}_{in} = \begin{bmatrix} A_0(\vec{\theta}) & A_1(\vec{\theta}) & A_2(\vec{\theta}) & A_3(\vec{\theta}) \end{bmatrix}_s \cdot \begin{bmatrix} S_0(\vec{\theta}) \\ S_1(\vec{\theta}) \\ S_2(\vec{\theta}) \\ S_3(\vec{\theta}) \end{bmatrix} \tag{4}$$

where $\underline{\mathbf{A}}_s$ is the system analyzer of the Stokes polarimeter, $\vec{\theta} = \{x \;\; y \;\; z \;\; t \;\; \sigma\}$ is a vector that includes the independent variables over which we modulate. Equation (4) can be further expanded as:

$$I_0(\vec{\theta}) = \sum_{i=0}^{3} A_i(\vec{\theta}) \cdot S_i(\vec{\theta}) \tag{5}$$

By applying Fourier transform onto Equation (5), it then becomes

$$\tilde{I}_0(\vec{\tilde{\theta}}) = \sum_{i=0}^{3} \tilde{A}_i(\vec{\tilde{\theta}}) * \tilde{S}_i(\vec{\tilde{\theta}}) \tag{6}$$

where $\vec{\tilde{\theta}} = \{\xi \;\; \eta \;\; \chi \;\; \nu \;\; \tau\}$ denotes the frequencies that correspond to $\vec{\theta}$ in the respective Fourier domain, $*$ represents convolution, and the tilde indicates the functions being Fourier transformed. For sinusoidal modulations, the Fourier transform $\tilde{A}_i(\vec{\tilde{\theta}})$ is a set of δ-functions. The Fourier transformed Stokes parameters are then convolved with these δ-functions which means the polarimetric information of the incident light are shifted to the location of these δ-functions in frequency space. The complete set of channels are therefore denoted as the *channel structure* of the system.[4]

A Q matrix is a matrix that collects the coefficients of Fourier transformed Stokes parameters of the intended channels. The Q matrix projects the incident Stokes parameters onto the intended channels in Fourier space. This process can be expressed as:

$$\underline{\mathbf{C}} = \underline{\underline{\mathbf{Q}}} \cdot \underline{\tilde{\mathbf{S}}} \tag{7}$$

Where Q is a $N_c \times 4$ matrix that maps the four Fourier transformed Stokes parameters into N_c number of channels. In frequency space, the Fourier transformed Stokes parameters can be un-mixed by applying the Q^{-1} to the intended channels.

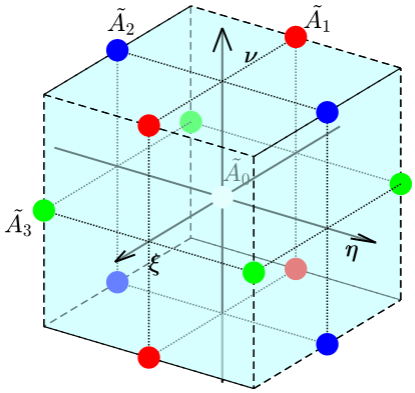

Figure 1: The chosen channel structure for building both multi-domain modulated polarimeters.The white dot represents the channel created by A_0, the red dots represent the channels created by A_1, the blue dots represent the channels created by A_2, the green dots represent by A_3

The Poincaré sphere provides an intuitive method to represent the polarizing effects of objects and polarization states of light. The Poincaré sphere is based on the normalized Stokes vectors,[14] which are designated $S_1/S_0, S_2/S_0$, and S_3/S_0. The normalized Stokes parameters are the three cartesian coordinates of a point in the Poincaré sphere: S_1 and S_2 are perpendicular to each other in the equatorial plane, and S_3 points toward the north pole of the sphere. Each point on the surface of the Poincaré sphere represents a unique polarization state with unity degree of polarization. Similar to the Stokes vector, analyzer vectors can also be illustrated using the Poincaré sphere. Therefore, the carrier generation elements in polarimeters will create certain trajectory on the Poincaré sphere. In this paper, we present a new type of multi-domain modulated polarimeter. In a conventional multi-domain modulated polarimeter, each of the carrier generating elements in the system can only affect the incident light beam in one domain. For this paper, we consider systems modulating in two domains (spatial and temporal) where $\vec{\theta} = \{x \;\; y \;\; t\}$ and $\vec{\tilde{\theta}} = \{\xi \;\; \eta \;\; \nu\}$.

For a conventional non-separable system, the system analyzer can be decomposed as equation (8):

$$\underline{\mathbf{A}}_s(x,y,t) = \underline{\mathbf{A}}(x,y,t) \cdot \underline{\underline{\mathbf{M}}}_1(x,y,t) \cdot \underline{\underline{\mathbf{M}}}_2(x,y,t) \cdots \underline{\underline{\mathbf{M}}}_n(x,y,t), \tag{8}$$

where $\underline{\mathbf{A}}_s$ is the system analyzer, $\underline{\mathbf{A}}$ is the separable analyzer in the system, $\underline{\underline{\mathbf{M}}}_n$ denotes the Mueller matrix of the nth modulating element. Separability implies that

$$\underline{\underline{\mathbf{M}}}_n(x,y,t) = \underline{\underline{\mathbf{M}}}_{n,1}(x,y) \cdot \underline{\underline{\mathbf{M}}}_{n,2}(t) \quad \text{or} \quad \underline{\underline{\mathbf{M}}}_n(x,y,t) = \underline{\underline{\mathbf{M}}}_{n,1}(t) \cdot \underline{\underline{\mathbf{M}}}_{n,2}(x,y) \tag{9}$$

On the other hand, the system analyzer in the new type of multi-domain system analyzed here can be decomposed as:

$$\underline{\mathbf{A}}_s(x,y,t) = \underline{\mathbf{A}}(x,y) \cdot \left(\underline{\underline{\mathbf{M}}}_1(x,y) \cdots \underline{\underline{\mathbf{M}}}_n(x,y)\right) \cdot \left(\underline{\underline{\mathbf{M}}}_1(t) \cdots \underline{\underline{\mathbf{M}}}_n(t)\right) \cdot \left(\underline{\underline{\mathbf{M}}}_1(x,y,t) \cdots \underline{\underline{\mathbf{M}}}_n(x,y,t)\right) \tag{10}$$

In conventional systems, as shown in Equation (8), the carriers imposed in the analyzer in different domains can be completely separated. In the new type of polarimeter, on the contrary, there exists carrier generating elements which generate non-separable carriers. Since the carriers in different domains are separable in the conventional system and not separable in the new system, they will be referred as separable polarimeters and non-separable polarimeters in this communication.

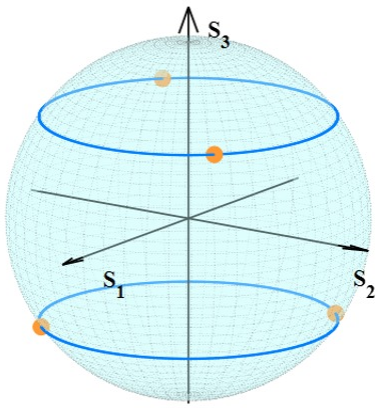

Figure 2: The analyzing states and the modulating trajectory of the designed multi-domain modulated Stokes polarimeter based on the chosen channel structure.

2. CHANNEL DESIGN

For a separable polarimeter, the analyzer optics create a channel structure where channels are located on a discrete orthogonal lattice with different amplitudes (i.e. the lattice vectors in the Fourier domain are all orthogonal to each other).[15] The channel cancellation method[4] helps the separable system to tune the amplitudes of unwanted channels to zero in order to increase the relative bandwidth of the intended channels, and the system as a whole. However, systematic errors in the system alter the amplitudes of the channels, causing some of the canceled channels to re-emerge and thus degrade the bandwidth of the useful channels. On the other hand, non-separable polarimeters create channels in diagonal directions in frequency space without the need for channel cancellation, and systematic error only alters the channel weights at the locations of the designed channels. To exhibit the advantages and disadvantages of separable polarimeters and non-separable polarimeters, both types of systems are designed based on the same channel structure. The channel structure investigated is shown in Fig.1.

This channel structure has several advantages. First, this channel structure measures all four Stokes parameters simultaneously. Second, each channel in this structure includes information from a single Stokes parameter. Third, this channel structure structure provides a relatively wider bandwidth of $\sqrt{2}/4 \cong 0.3536$ cycles per sample comparing to similar channel structures.[9] The analyzer vector corresponding to this channel structure is:[9]

$$\begin{bmatrix} 1 & \frac{1}{\sqrt{3}}\cos(\pi(x+t)) & \frac{1}{\sqrt{3}}\cos(\pi(y+t)) & \frac{1}{\sqrt{3}}\cos(\pi(x+y)) \end{bmatrix} \tag{11}$$

In practice, and when sampled at Nyquist, this analyzer vector results in the following four vectors repeating spatially and temporally,[4]

$$\begin{bmatrix} 1 \\ \frac{-1}{\sqrt{3}} \\ \frac{-1}{\sqrt{3}} \\ \frac{1}{\sqrt{3}} \end{bmatrix}, \begin{bmatrix} 1 \\ \frac{1}{\sqrt{3}} \\ \frac{-1}{\sqrt{3}} \\ \frac{-1}{\sqrt{3}} \end{bmatrix}, \begin{bmatrix} 1 \\ \frac{-1}{\sqrt{3}} \\ \frac{1}{\sqrt{3}} \\ \frac{-1}{\sqrt{3}} \end{bmatrix}, \begin{bmatrix} 1 \\ \frac{1}{\sqrt{3}} \\ \frac{1}{\sqrt{3}} \\ \frac{1}{\sqrt{3}} \end{bmatrix} \tag{12}$$

On the Poincaré sphere, these repeating analyzer vectors correspond to four symmetric points as shown in Fig. 2. The modulation system that can achieve this channel structure must has an analyzer vector forming a trajectory that can cover these four points and can be controlled to take only these four points in sequence on the Poincaré sphere.

3. SYSTEM DESIGN

Based on the trajectory and the limited analyzing states on the Poincaré sphere, both separable and non-separable systems are designed to generate the desired channel structure. The separable system consists of a detector, a

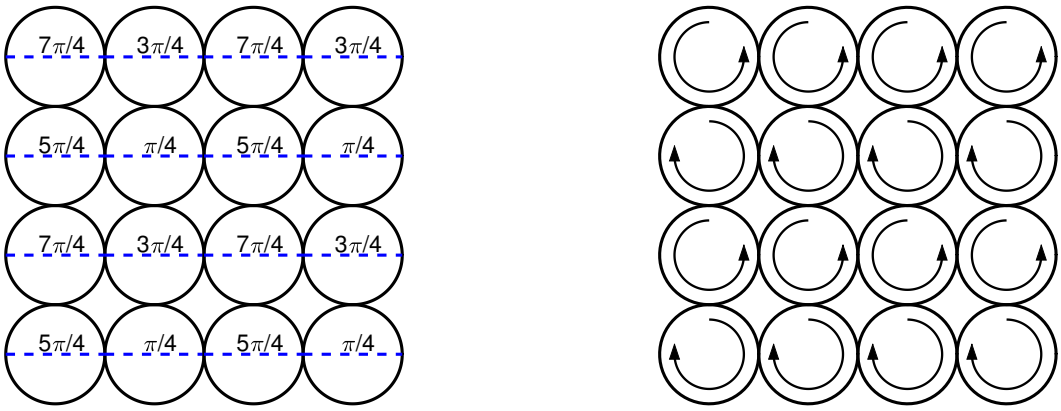

(a) Micro Linear Retarder Array (linear MRA) (b) Micro Circular Retarder Array (circular MRA)

Figure 3: Micro retarder arrays in the seprable system

linear polarizer, a micro circular retarder array (MRA), a micro linear retarder array (MRA), and a rotating half waveplate. From the light beam entrance to the detector, the modulating elements are arranged in the following sequence: a rotating half waveplate, a linear MRA, a circular MRA and a linear polarizer. In practice, the half waveplate rotates 45° for each sampling while the linear polarizer maintain horizontal direction.

The linear MRA is tiled with the retardance of $\frac{7\pi}{4}$, $\frac{5\pi}{4}$, $\frac{3\pi}{4}$ and $\frac{\pi}{4}$ rad, as shown in Fig. 3a. The numbers in the figure denote the retardance of the corresponding micro waveplate and the dash lines indicate their fast axes.

The circular MRA consists of left circular retarders with retardance of $\cos^{-1}(\frac{1}{\sqrt{3}}) \cong 0.9553$ rad and right circular retarders with retardance of $\pi - \cos^{-1}(\frac{1}{\sqrt{3}}) \cong 2.1863$ rad. The micro left circular waveplates and micro right circular waveplates are arranged in the pattern shown in Fig. 3b.

The non-separable system consists of a detector, a micro polarizer array, a quarter waveplate and a "non-separable" element. These elements are assembled in sequence: the incident light first interacts with the "non-separable" element before being passed through the stationary quarter waveplate, then filtered by a linear micro polarizer array(MPA), and finally measured by the detector. The MPA used here consists of repeating 45° and 135° polarizers as shown in Fig.4. Note that this MPA pattern has significant resemblance with the $2 \times 2 \times 2$ and $2 \times 2 \times 3$ MPAs introduced by Alenin.[16,17]

The "non-separable" element is a micro linear retarder array where each micro linear retarder is rotatable. All micro retarders have the same retardance of $\cos^{-1}(\frac{1}{\sqrt{3}}) \cong 0.9553$ rad. The "non-separable" element is designed to modulate the incident light beam in both spatial and temporal domains. Therefore, the micro retarders

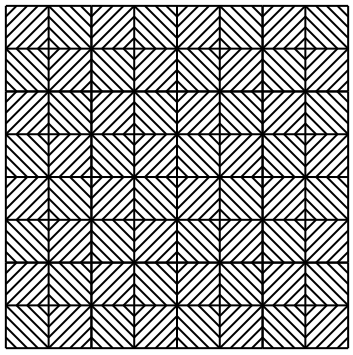

Figure 4: The micro polarizer array in the non-separable system, 45° and 135° micro linear polarizers are repeatedly tiled as in the presented pattern.

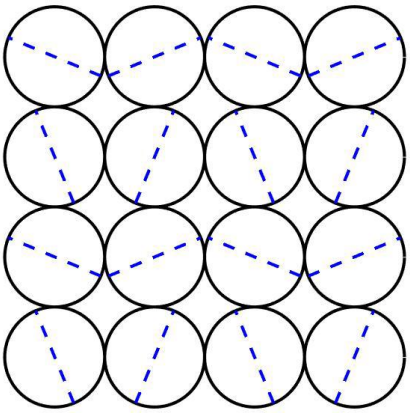

Figure 5: The "non-separable" element (rotatable micro retarder array). The dashed lines in the figure denotes the fast axes.

initially orient their fast axis at 157.5°, 112.5°, 22.5° and 67.5° repeatedly and rotate 90° for each sampling time. The physical design of the "non-separable" element is as illustrated in Fig. 5. Although the "non-separable" modulating optic do not exist presently, there are potential candidate devices that may be able to generate the desired set of carriers. For example, Brodzeli et al[18] introduced a fully integrated polarization-based photonic transducer which exhibits fast response to an applied electric field, and this can in principle allow a pixel-by-pixel addressable access to the entire Poincarè sphere.

Although two systems are constructed to generate the same final channel structure, these two channel structures are inherently different. As mentioned in Section 2, the separable system has a set of channels located on the rectangular lattice. By adjusting the parameters of the optics in the system, many of these are canceled, resulting in the structure desired. Fig.6a shows an example of varying the retardance of the half waveplate of the

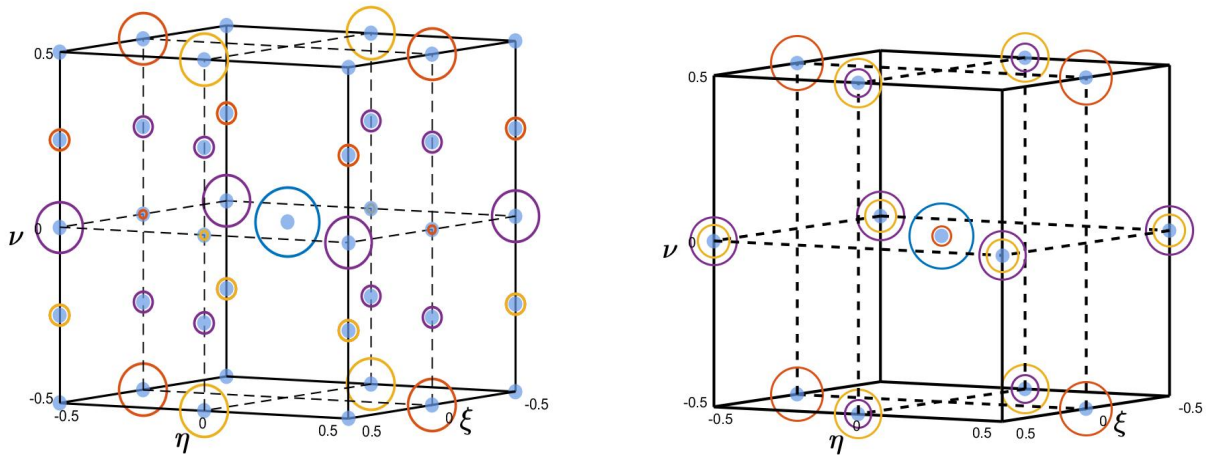

(a) The channel structure of the separable system when the retardance of the half waveplate changes.

(b) The channel structure of the non-separable system when the retardance of the quarter waveplate changes.

Figure 6: An example of how the channel structures change when the retardance of wavplates changes in both system. The light blue dots are potential channel locations. The blue, red, yellow, purple circles are channels created by A_0, A_1, A_2 and A_3 respectively.

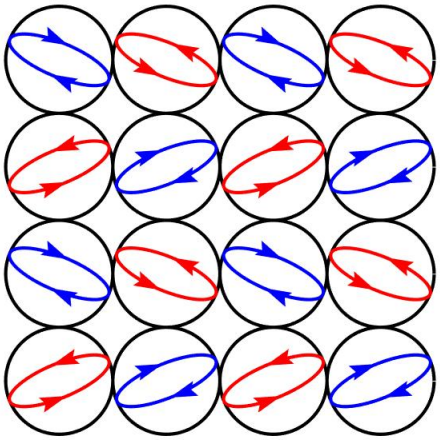

Figure 7: The analyzing state of both system when no systematic error exists.

separable system to obtain the designed channel structure. On the other hand, the channels generated by the non-separable system locate in the diagonal directions without creating the redundant channels which locate in rectangular lattices. An example showing how the channel structure changes when the retardance of the quarter waveplate of the non-separable system changes is presented in Fig.6b.

4. SIMULATION

This section describes the simulation results of the two Stokes polarimeters considered in this paper. First simulations are done assuming there is no systematic error or noise in either system. Then, simulations are done by adding systematic errors into each elements in both systems. By comparing the simulation results, some preliminary conclusion about the advantages and disadvantages of both types of polarimeters are drawn.

At the very sampling rates mentioned before and in absence of systematic errors, both systems will have identical analyzer vectors since they share the same designed channel structure. Fig. 7 depicts the analyzing states of each pixel. The blue and red ellipses indicate the analyzing states are right-handed or left-handed. And for each sampling, these ellipses rotate as the analyzer vectors varying. In the simulation, the polarimetric data

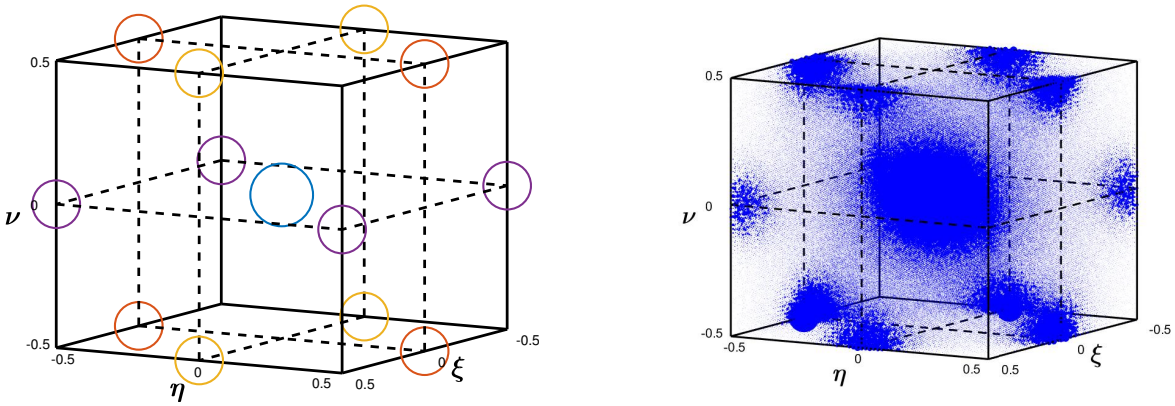

(a) Simulated channel structure (b) Simulated Fourier space

Figure 8: Simulated channel space of both systems when no systematic error occurs

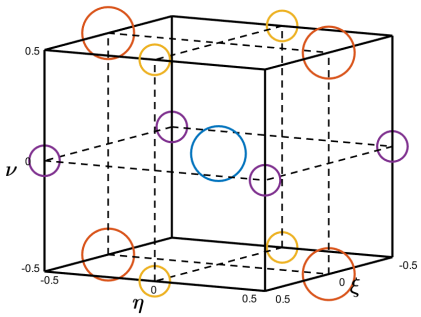

(a) When retardance errors added into the circular MRA.

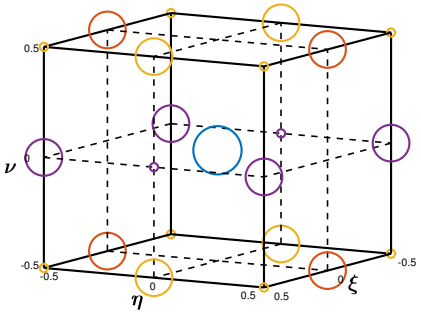

(b) When retardance errors added into the linear MRA.

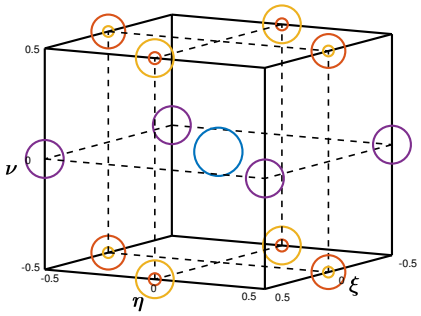

(c) When angular errors added into the linear MRA.

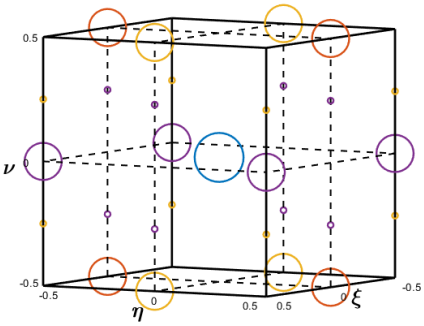

(d) When retardance errors added to the rotating half waveplate.

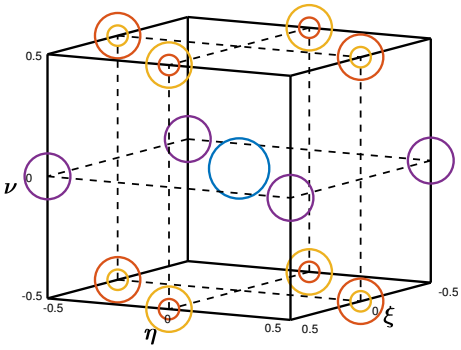

(e) When angular errors added to the rotating half waveplate.

Figure 9: Channel structure of the separable system when systematic errors are added

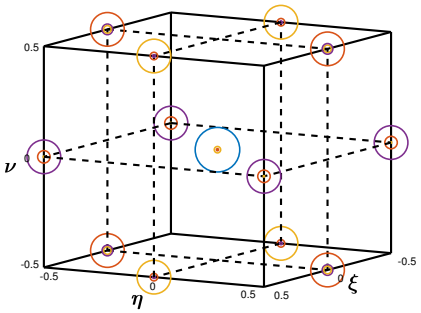

(a) When the "settled" errors are added

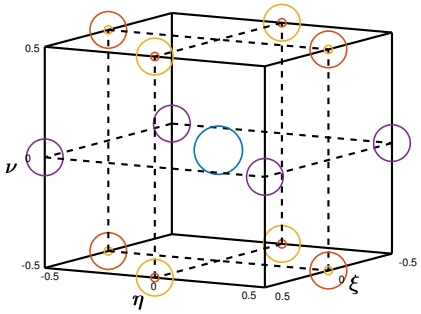

(b) When the "varying" errors are added

Figure 10: Channel structure of the non-separable system when systematic errors are added

we used were generated following a power law PSD spatio-temporally.[19] As the simulation shows, in the channel space, the Fourier transformed polarimetric data were distributed into the desired channels.

The simulation results are presented in Fig. 8. Fig. 8a indicates the channel structure of both systems: the blue, red, yellow and purple circles represent the channels created by the analyzer parameter A_0, A_1, A_2 and A_3 respectively. The volumes of the circles indicate the amplitudes of the channels. Fig. 8b is the actual simulated Fourier space of the modulation systems. The band limited polarimetric data are Fourier transformed and assigned into the corresponding channels.

When systematic errors are added into both systems, the ideal channel structure is degraded. However, since the modulation schemes of the two types of Stokes polarimeters are different, the distorted channel structures and the influence of the systematic errors are different. The systematic errors include: manufacturing errors of the modulation optics and control errors of the moving parts of the modulation systems. In Stokes polarimeters, the manufacturing errors include: the retardance and angular deviations in the waveplate, the linear polarizer, the micro polarizer arrays and the micro retarder arrays. The controlling errors means the errors generated by the imprecise positioning of the moving parts in the modulation systems. To be more specific, the controlling errors are the angular errors of the rotating waveplates.

In the simulation of the separable system, the linear polarizer is assumed to be perfect since it is not hard to find a commercial polarizer with high extinction ratio. In addition, the polarizer is assumed to precisely orient at the horizontal direction through calibration. The circular MRA has only retardance errors since there is no fast axis in circular waveplates. In the simulation, the retardance error of the circular MRA was generated randomly with a normal distribution. Fig.9a shows the retardance error of the circular MRA causes the varying of the amplitude of the channels in the Fourier domain. The linear MRA has both "settled" angular and retardance error (both errors obey normal distribution) and they cause different effects in the channel space. The angular errors will create extraneous channels locate at the designed positions of $\tilde{A}_1$ and $\tilde{A}_2$ as shown in Fig. 9c. On the other hand, the retardance error of the linear MRA would created channels in between the originally designed channels as Fig. 9b. The rotating half waveplate in the separable system has two potential error sources: the retardance error and the angular error from the rotation. The simulation shows the retardance error of the rotating half waveplate also creates extraneous channels locates in between the desired channels as shown in Fig. 9d. The simulation result is shown in Fig.9e when rotating angular errors are added to the rotating half waveplate. In the frequency space, if the extraneous channels are not varying randomly and sit at the location of the intended channels, they are easily calibratable with the Q-matrix method. But the extraneous channels located in between the designed channels and the "varying" channels cannot be treated in the same way and may tarnish the performance of the separable system by decreasing channel bandwidth and creating potential channel crosstalk.

The simulated PSNR results of the separable system are shown in Fig.11a and Fig.11b. The extraneous channels located between designed channels did not cause much decrease in PSNR, since the Stokes parameters are band limited and these channels are tiny comparing to the desired channels in this case, as Fig. 11a shows. However, these tiny channels put a limit to the channel filters and the bandwidth of the desired data. The PSNR value of the system may decline severely if the data have a wider bandwidth or if the channel filters are not carefully chosen. As for the "varying" errors, since they are not calibratable, in this system, they will degrade the reconstruction of S_1 and S_2 data.

In the non-separable system, there are three main modulation optics: the MPA, the stationary waveplate and the "non-separable" element. For the MPA, the errors include the angular error and the transmission error of each micro polarizer. Here, only the angular error is considered since it is not hard to find commercial MPA with high extinction ratio. In the simulation, the angular error of the MPA obeys normal distribution. Only retardance deviation is considered in the stationary waveplate. The retardance deviation was generated randomly within the tolerable error range of normal commercial waveplates. The "non-separable" element has three error sources: the retardance deviation at each pixel, the initial angular deviation (before the fast axes rotate), and the rotating angular deviation (the rotation accuracy). The angular and retardance errors of the non-separable element are sampled from a normal distribution. In the non-separable system, the systematic errors cause one main effect: some systematic errors created channels mixed into the locations designed for desired channels as shown in Fig.10.

The main negative effects caused by the manufacturing systematic errors are the emerging unintended channels locate at the positions of the desired channels. Since these errors are not variable, the corresponding

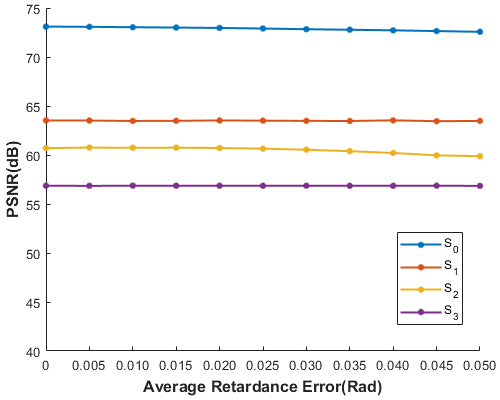

(a) Separable system performance when extraneous channels emerge in the channel space

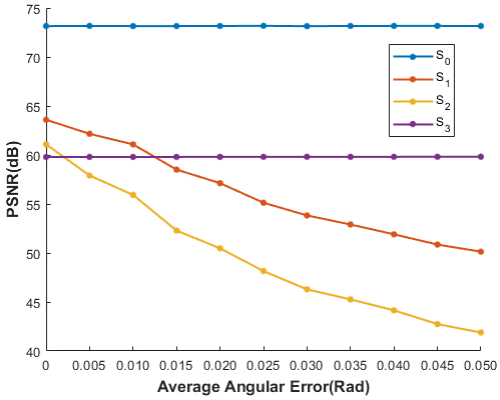

(b) Separable system performance when the "varying" error occurs

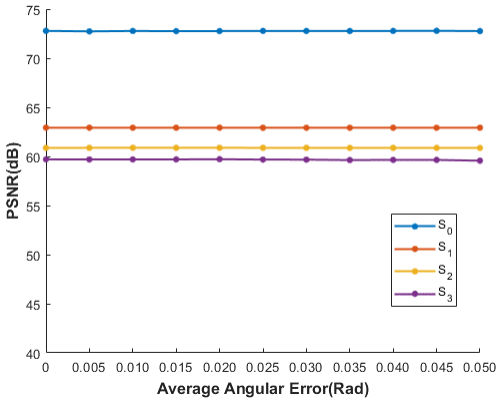

(c) Non-separable system performance when Q-matrix method is applied

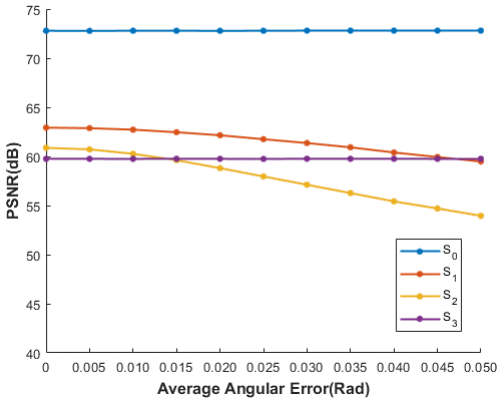

(d) Non-separable system performance when the "varying" error occurs

Figure 11: PSNR comparison

extraneous channels are also fixed. And therefore, the resulting channel structure can be calibrated mathematically using the Q-matrix method. However, the angular errors generated by the rotation of micro waveplates of the "non-separable" element cannot be dealt with by the same method since these errors are varying and random during the sampling process. Fig.10b shows the channel structure of the non-separable system when these "varying" errors are added into the system. Therefore, the quality of the reconstructed images of the non-separable system depends on how strong the "varying" errors are in the system. Fig.11c and Fig.11d shows the simulated PSNR performance of the non-separable Stokes polarimeter.

As Fig.11c shows, calibrated by the Q-matrix method, the non-separable system has a high-level and stable PSNR performance if only "settled" errors exist in the system. On the other hand, the "varying" errors will tarnish the reconstruction of S_1 and S_2 data (Fig.11d).

Comparing Fig. 11d to Fig. 11b, the separable system experience a more significant PSNR decline when the "varying" error occur. This effect is caused by the mathematical complexity of the separable system. In the non-separable system, the errors stay in the sinusoidal functions in the Mueller matrix of the non-separable element. In contrast in the separable system, the errors in the Mueller matrix of the rotating half waveplate are amplified by the Mueller matrices of the following elements.

5. CONCLUSION

In this study, both separable and non-separable multi-domain modulated Stokes polarimeters are designed to realize the same channel structure. This specific channel structure is chosen because (1) it provides a relatively higher channel bandwidth in the Fourier domain. (2) it measures all four Stokes parameters simultaneously. (3) the Stokes parameters are separated in all the channels. The performance of both systems are simulated when systematic errors are added into the systems and the performance of both systems are evaluated by their PSNRs. The simulation results of both systems are then compared. The non-separable system shows an advantage over the separable system. Under the same level of instrument performance, the quality of the data reconstruction of the separable system is constrained by the noncalibratable extraneous channels located between the designed channels. The non-separable system, on the other hand, has all the error-created extraneous channels located at the designed channels. Therefore, the additional bandwidth constraint does not exist in the non-separable system. Further more, comparing to the separable system, the non-separable system exhibits a considerably smaller decrease in PSNR when the noncalibratable "varying" errors occur.

REFERENCES

[1] Oka, K. and Kato, T., "Spectroscopic polarimetry with a channeled spectrum," *Optics Letters* **24**(21), 1475–1477 (1999).

[2] Hagen, N., Oka, K., and Dereniak, E. L., "Snapshot mueller matrix spectropolarimeter," *Optics letters* **32**(15), 2100–2102 (2007).

[3] Kudenov, M. W., Escuti, M. J., Hagen, N., Dereniak, E. L., and Oka, K., "Snapshot imaging mueller matrix polarimeter using polarization gratings," *Optics letters* **37**(8), 1367–1369 (2012).

[4] Vaughn, I. J., *Bandwidth and Noise in Spatio-temporally Modulated Mueller Matrix Polarimeters*, PhD thesis, Uni. of AZ (2016).

[5] LaCasse, C. F., Chipman, R. A., and Tyo, J. S., "Band limited data reconstruction in modulated polarimeters," *Optics Express* **19**(16), 14976–14989 (2011).

[6] Alenin, A. S. and Tyo, J. S., "Generalized channeled polarimetry," *JOSA A* **31**(5), 1013–1022 (2014).

[7] Snik, F., Craven-Jones, J., Escuti, M., Fineschi, S., Harrington, D., De Martino, A., Mawet, D., Riedi, J., and Tyo, J. S., "An overview of polarimetric sensing techniques and technology with applications to different research fields," in [*Polarization: Measurement, Analysis, and Remote Sensing XI*], **9099**, 90990B, International Society for Optics and Photonics (2014).

[8] Snik, F., Van Harten, G., Alenin, A. S., Vaughn, I. J., and Tyo, J. S., "A multi-domain full-stokes polarization modulator that is efficient for 300-2500nm spectropolarimetry," in [*Polarization Science and Remote Sensing VII*], **9613**, 96130G, International Society for Optics and Photonics (2015).

[9] LaCasse, C. F., Ririe, T., Chipman, R. A., and Tyo, J. S., "Spatio-temporal modulated polarimetry," in [*Polarization Science and Remote Sensing V*], **8160**, 81600K, International Society for Optics and Photonics (2011).

[10] Vaughn, I. J., Rodríguez-Herrera, O. G., Xu, M., and Tyo, J. S., "A portable imaging mueller matrix polarimeter based on a spatio-temporal modulation approach: theory and implementation," *Proc. SPIE* **9613**(961304), 961304 (2015).

[11] Vaughn, I. J., Rodríguez-Herrera, O. G., Xu, M., and Tyo, J. S., "Bandwidth and crosstalk considerations in a spatio-temporally modulated polarimeter," *Proc. SPIE* **9613**(961305), 961305 (2015).

[12] Vaughn, I. J., Alenin, A. S., and Tyo, J. S., "A fast stokes polarimeter: preliminary design," in [*Polarization Science and Remote Sensing VIII*], *Proc. SPIE* **10407**, 1040702, International Society for Optics and Photonics (2017).

[13] Goldstein, D. H., [*Polarized light*], CRC press (2017).

[14] Collett, E., [*Field guide to polarization*], vol. 15, SPIE press Bellingham (2005).

[15] Vaughn, I. J., Alenin, A. S., and Tyo, J. S., "Focal plane filter array engineering I: rectangular lattices," *Opt. Express* **25**(10), 11954–11968 (2017).

[16] Alenin, A. S., Vaughn, I. J., and Tyo, J. S., "Optimal bandwidth micropolarizer arrays," *Optics letters* **42**(3), 458–461 (2017).

[17] Alenin, A. S., Vaughn, I. J., and Tyo, J. S., "Optimal bandwidth and systematic error of full-stokes micropolarizer arrays," *Applied optics* **57**(9), 2327–2336 (2018).

[18] Brodzeli, Z., Silvestri, L., Michie, A., Guo, Q., Pozhidaev, E. P., Chigrinov, V., and Ladouceur, F., "Sensors at your fibre tips: a novel liquid crystal-based photonic transducer for sensing systems," *Journal of Lightwave Technology* **31**(17), 2940–2946 (2013).

[19] Vaughn, I. J., Alenin, A. S., and Tyo, J. S., "Statistical scene generation for polarimetric imaging systems," *arXiv preprint arXiv:1707.02723* (2017).